Japanese Journal of Applied Physics

The Japan Society of Applied Physics

REGULAR PAPER

Improvement of piezoelectric properties of relaxor type $0.695Pb(Mg_{1/3}Nb_{2/3})O_3{-}0.305\ PbTiO_3$ single crystal plate and silver vibrator by alternating current poling

Japanese Journal of Applied Physics 61, SN1009 (2022) **REGULAR PAPER**
https://doi.org/10.35848/1347-4065/ac7c52

Check for updates

Improvement of piezoelectric properties of relaxor type 0.695Pb($Mg_{1/3}Nb_{2/3}$)O_3–0.305 $PbTiO_3$ single crystal plate and silver vibrator by alternating current poling

Zhuangkai Wang[1], Yohachi (John) Yamashita[1,2], Yiqin Sun[1], Tadashi Fujii[1], and Tomoaki Karaki[1*]

[1]Faculty of Engineering, Toyama Prefectural University, Imizu, 9390398 Toyama, Japan
[2]Mechanical & Aerospace Engineering, North Carolina State University, Raleigh, NC 27695-7910, United States of America

[*]E-mail: chen@pu-toyama.ac.jp

Received June 11, 2022; accepted June 26, 2022; published online July 22, 2022

Alternating current poling (ACP) and direct current poling (DCP) on [001]-oriented 0.695Pb($Mg_{1/3}Nb_{2/3}$)O_3–0.305$PbTiO_3$ (PMN-0.305PT) single crystal (SC) plates with a dimension of 12 × 4 × 0.3 mm and silver vibrators of 12 × 0.15 × 0.3 mm were investigated. The highest dielectric constant of 14500 and piezoelectric constant of 4200 pCN^{-1} were confirmed with the ACP SC plate manufactured by the conventional one charge Bridgman process. After array dicing into silver, the silver mode coupling coefficient k'_{33} = 94.3% was obtained from ACP SC. However, many spurious mode vibrations (SMV) were seen in the impedance spectra of the DCP and ACP SC silver vibrators. We consider that this SMV may be caused by array dicing damage. The PMN-0.305PT SC plate near the morphotropic phase boundary shows excellent piezoelectric and dielectric properties, however, these silvers tend to show SMV after dicing. This information is useful to select the PMN-PT composition for medical probe application.

1. Introduction

Relaxor-based ferroelectric single crystals (SC), such as (1-x) Pb($Mg_{1/3}Nb_{2/3}$)O_3–$x$$PbTiO_3$ (PMN–xPT), have attracted great attention for applications in sensors, transducers, imaging devices, and actuators due to their excellent piezoelectric and electromechanical properties ($d_{33} > 2000$ pCN^{-1}, $k_{33} > 90\%$).[1–4] Shrout et al. investigated PMN-xPT exhibiting a superb piezoelectric constant d_{33} value of more than 1500 pCN^{-1} when the x composition is around 30 mol%,[5] and the PMN-xPT SC system with compositions near the morphotropic phase boundary (MPB) has particularly drawn interesting research.[6] It has been reported that the MPB region ($0.30 < x < 0.35$) contains low-symmetry monoclinic (M) phases, separating rhombohedral (R) and tetragonal (T) phases, and this multiphase coexistence flattens the free-energy profile of polarization rotation between the R and T phases, playing a key role in the giant piezoelectric response.[7,8)

Recently, high-frequency (>10 MHz) ultrasonic imaging has been widely used in diagnostics of eyes, skin, and blood vessels, etc.[9–11] In order to obtain clearer ultrasonic imaging, high-frequency ultrasonic transducers with broad bandwidth and high resolution are required. Therefore, increasing the working frequency and the number of elements are the main development trends of medical ultrasonic transducers. In addition, in the current application for ultrasonic diagnosis, most equipment is cart type and heavy, so that it cannot be moved easily for use. Therefore, the development of small-scale mobile ultrasonic equipment is another trend.[12] High-quality relaxor-based SCs, such as PMN-0.30PT, have been considered promising materials for medical ultrasonic imaging application, and suitable for miniaturized transducer applications due to their outstanding piezoelectric and dielectric properties.[13,14] Furthermore, major ultrasonic imaging companies have started using the PMN-PT SC for two-dimensional array probes for medical imaging applications.[15]

For ferroelectric-based piezoelectric materials which are macroscopically piezoelectric, poling is an indispensable process to align randomly-distributed domains and thus obtain high piezoelectric and dielectric properties. Direct current poling (DCP) has been widely used for such domain-controlling processes. However, since the first demonstrations of a dynamic alternating current poling (ACP) by Yamamoto and Yamashita et al., it has been considerably important due to its further enhancements in dielectric and piezoelectric properties.[16,17] So far, more than 40 papers relevant to ACP have been reported in the past few years.[18–38]

Li et al. reported that the Sm-doped PMN-0.30PT SC possesses giant piezoelectricity over 4100 pCN^{-1} and free dielectric permittivity ($\varepsilon_{33}{}^{T}/\varepsilon_0$) of 12500 in 2019.[37] In this work, we investigated ACP effects on dielectric and piezoelectric properties of plate and silver vibrators of PMN-0.305PT SC manufactured by a conventional one-charge Bridgman process.

2. Experimental procedure

Figure 1 shows schematic illustrations of (a) the traditional one charge Bridgman method in which compositional segregations naturally occur during crystal growth, (b) [001]-oriented PMN-0.305PT wafer cut into rectangular plates with dimensions of $L12 \times W4 \times T0.3$ mm and (c) thin silver mode vibrator with dimensions of $L12 \times W$ $0.15 \times T$ 0.3 mm cut form plates shown in (b) after poling treatment.

Since the absolute value of the alternating current (AC) voltage varies with its waveform, we adopted root mean square (rms) voltages for ACP conditions in order to compare with direct current (DC) voltages. The term “rms voltage” also known as the effective or heating value of AC is associated with the generation of identical heat at the same time in a resistor. Thus, the AC voltages could be properly compared with the DC voltages.

The PMN-0.305PT SC plates were treated by ACP at 40 °C using bipolar sine waves in the air. The poling electric field was 8 kV rms cm^{-1} with a frequency of 50 Hz and was repeated for 50 cycles. To compare with the ACP effect, we also conducted DCP in the air with a temperature of 40 °C, and the electric field was 8 kV cm^{-1} and lasted for 5 min during the poling procedure. In addition, the plate samples after poling 48 h were cut into thin silver vibrators as shown in Fig. 1 (c) by a

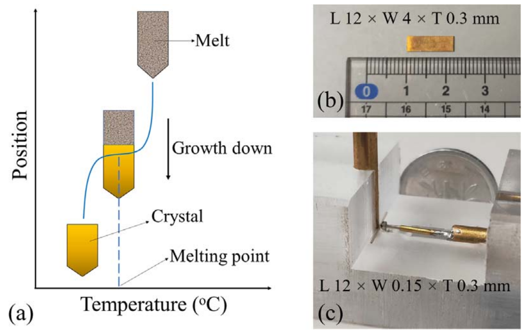

Fig. 1. (Color online) (a) Conventional one charge Bridgman method for manufacturing PMN-PT SC ingot. (b) the PMN-0.305PT rectangular plate with sputtering 50 nm Cr/200 nm Au electrodes. (c) the PMN-0.305PT thin silver mode vibrator with the width and thickness ratio of 2.0.

0.05 mm diamond blade of the dicing saw (DISCO Co., DAD 3350 Tokyo, Japan) at an array dicing speed of 1.0 mm s^{-1}.

Both these plates and silvers of PMN-0.305PT SC were measured for their electric capacitance by an impedance analyzer (HP 4194 A, USA) at 1 kHz and at two times the anti-resonant frequency ($2f_a$), respectively. Thus, the $\varepsilon_{33}{}^{T}/\varepsilon_0$ and clamped dielectric permittivity ($\varepsilon_{33}{}^{S}/\varepsilon_0$) were calculated. The electromechanical coupling coefficient of length mode vibration (k_{31}) and thickness mode vibration (k_t) were obtained according to the following Eqs. (1) and (2).

$$k_{31} = \sqrt{\frac{r}{r - \tan r}}, \text{ in which}$$

$$r = \frac{\pi}{2} \cdot \frac{f_a}{f_r} \,(f_r \text{ is the resonant frequency}) \tag{1}$$

$$k_t = \sqrt{\left(\frac{\pi}{2} \cdot \frac{f_r}{f_a}\right) \cot\left(\frac{\pi}{2} \cdot \frac{f_r}{f_a}\right)} \tag{2}$$

Although the piezoelectric constant d_{33} of PMN-0.305PT plate could be directly measured by the d_{33} meter (MODEL ZJ-4BN), that of the silver mode vibrator could only be calculated by Eq. (3) due to its fragility.

$$d_{33} = k_{33}\sqrt{\frac{\varepsilon_{33}^{T}}{Y^E}} \quad (Y^E \text{ is Young's modulus}) \tag{3}$$

Furthermore, the temperature dependence of $\varepsilon_{33}{}^{T}/\varepsilon_0$ and loss (TDDP&L) for PMN-0.305PT SC plates at 1 kHz were obtained by a computer-controlled LCR meter (Hioki IM-3570, Japan) at every 0.1 °C in a temperature range of 25 °C–250 °C.

We also conducted structural analyses after poling by X-ray diffraction (XRD) (Rigaku Corp., RINT 2200 model, Japan) with CuKα_1 monochromatic radiation. The (004) peaks of PMN-0.305PT after ACP and DCP were measured at room temperature.

3. Result and discussion

The value of d_{33} of PMN-0.305PT SC plates after ACP and DCP at 25 °C were 4200 pCN^{-1} and 2800 pCN^{-1} as shown in Figs. 2(a) and 2(b), respectively. The d_{33} of the ACP plate was about 50% higher than that of the DCP, indicating that the appropriate ACP condition could greatly enhance the dielectric properties of PMN-30.5PT. Figure 2(c) presented how the $\varepsilon_{33}{}^{T}/\varepsilon_0$ and dielectric loss change with time after ACP and DCP. In the period time from 10 h to 1000 h, when the samples after poling were in a relatively stable state, we calculated the aging of the $\varepsilon_{33}{}^{T}/\varepsilon_0$ of the sample. The high-performance ACP sample showed a high aging rate of 4.3%/decade, which was about twice that of the DCP sample. Both ACP and DCP samples' dielectric loss decreased rapidly within 10 h, but the changes were no longer obvious after 10 h.

Table I shows dielectric and piezoelectric properties of various relaxor-PT SCs after ACP comparing this work. It is worthy to note that the highest $\varepsilon_{33}{}^{T}/\varepsilon_0$ and d_{33} values of PMN-0.305PT were confirmed as shown in this table.

The TDDP&L of PMN-0.305PT SC plate by ACP and DCP treatments is shown in Fig. 3. It has been reported that the PMN-0.305PT composition near MPB is monoclinic by many researchers.[3,39] Therefore, according to Fig. 3, we inferred that the phase transition path of DCP PMN-0.305PT SC are 77 °C for M_B (or M_A) →M_C, 86 °C for M_C → T and 142 °C for T → C. In contrast, ACP samples showed similar but slightly different phase transition temperatures near 90 °C. The first $\varepsilon_{33}{}^{T}/\varepsilon_0$ drop is at 67 °C from M_B (or M_A) to M_C, which is 10 °C lower than that of DCP samples. Unlike DCP samples, there was almost no upward trend after the first $\varepsilon_{33}{}^{T}/\varepsilon_0$ drop, the $\varepsilon_{33}{}^{T}/\varepsilon_0$ of ACP samples increased rapidly and reached a peak at 90 °C. In addition, in the range from 90 °C to Curie temperature (T_c), the $\varepsilon_{33}{}^{T}/\varepsilon_0$ of ACP samples always remained above 20,000, which is much greater than that of DCP samples. It demonstrates that the different poling conditions lead to the different phase transition sequence during the heating process.

Figure 4 shows impedance spectra and phases of DCP and ACP plates sample. The DCP SC plate showed no SMV, however, the ACP SC plate showed several SMV between f_r and f_a. The calculated k_{33} of the ACP plate sample was up to 96.5% and that of the DCP plate sample was up to 95.1%.

Due to the excellent piezoelectric and dielectric properties of the ACP plate samples, we decided to dice them into silver mode vibrators, test their properties, and compare with these plate samples. As shown in Fig. 5(a), the coupling factor k'_{33} of 94.3% for silver mode vibrators was confirmed. However, it also shows the presence of small SMV on its impedance, which may be due to the large amount of heat generated during dicing and/or overpoling effects of the plate sample.[38] We also tried to depole the silver samples by heating them over T_c and repole them to eliminate these SMV, however, it was not successful to eliminate these SMV after many trials. Figure 5(b) shows the variation of k'_{33} and k_{31} mode vibrations of the silver ACP and DCP samples as a function of temperature for every 5 °C to 100 °C increase. The k'_{33} of the ACP samples decreased significantly at 40 °C, remained stable in the range of 50 to 75 °C, and finally started to rebound at 90 °C, which seemed to be inconsistent with the TDDP&L of the plate samples as shown in Fig. 3. This indicated that even if the poling conditions of the plate sample and the 0.15 mm silver sample were same, the dielectric properties may be significantly different. However, the mechanism of this phenomenon needs more intensive work in the future.

Table II shows comparison of plate and silver mode vibrators' dielectric and piezoelectric properties. According to the table, both piezoelectric constant d_{33} and $\varepsilon_{33}{}^{T}/\varepsilon_0$ of

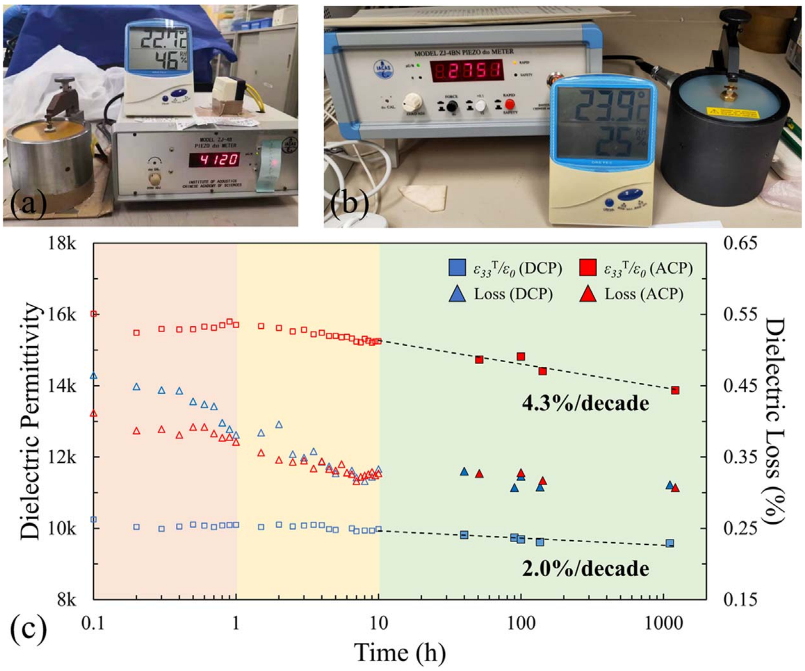

Fig. 2. (Color online) (a) the piezoelectric coefficient d_{33} value of PMN-0.305PT plate after ACP treatment and (b) that after DCP treatment, and (c) the aging of $\varepsilon_{33}{}^T/\varepsilon_0$ and dielectric loss after poling.

Table I. Dielectric and piezoelectric properties of various relaxor-PT SCs after ACP.

Sample	$\varepsilon_{33}^T/\varepsilon_0$ (25 °C)	tan δ (%)	d_{33} (pCN^{-1})	k_t (%)	References
0.75PMN-0.25PT	6397	/	1730	55–57	18
0.70PMN-0.30PT	8500	/	1980	57	20
0.70PMN-0.28PT	8900	0.31	2430	58.1	28
0.24PMN-0.46PIN-0.30PT	7000	0.59	2340	59.3	34
0.52PMN-0.15PYbN-0.33PT	6800	1.1	2490	57	24
Sm-0.7PMN-0.3PT	12500	1.0	4100	/	37
0.695PMN-0.305PT	14500	0.34	4200	59.5	This work

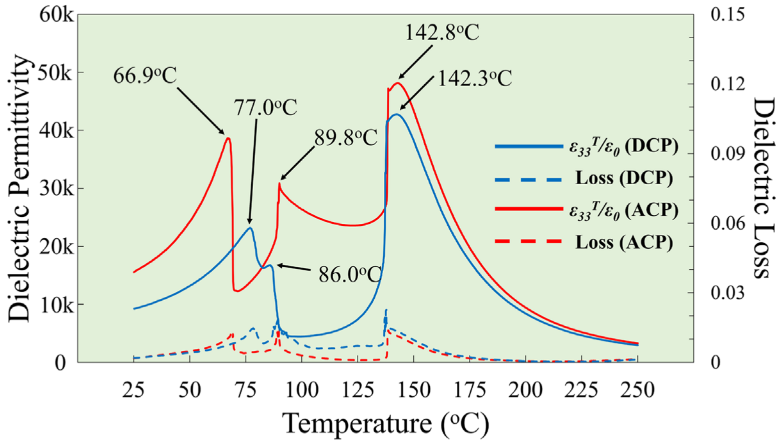

Fig. 3. (Color online) The TDDP&L of PMN-0.305PT SC plate by ACP and DCP treatments.

silver mode vibrator were drastically decreased (over 50%) after dicing from the plate sample. One of our future works is enhancing the dielectric properties of silver mode SC vibrators by selecting optimal dicing condition.

The XRD result of (004) peak intensity of PMN-0.305PT plate samples by ACP and DCP were shown in Fig. 6. As mentioned above, it has been reported that the PMN-0.305PT composition is monoclinic.[3,39] Besides, recently, PMN-0.26PT and Mn-doped $Pb(In_{1/2}Nb_{1/2})O_3$-$Pb(Mg_{1/3}Nb_{2/3})O_3$-$PbTiO_3$ (PIN-PMN-PT) are originally 4 R (4 rhombohedral domain configuration) after DCP along the [001] direction. Due to ACP, the 71° domain disappeared, and the theory that 4 R turned into 2 R has been reported.[40,41] Therefore, we speculated that the PMN-0.305PT SC is 4 M (4 monoclinic domain configuration) by DCP and it changes to 2 M by ACP. Moreover, the XRD of the ACP samples shifted to high angles, indicating that the lattice constant of the *c*-axis was smaller than that of the DCP samples, so we inferred that this 2 M is very close to the R

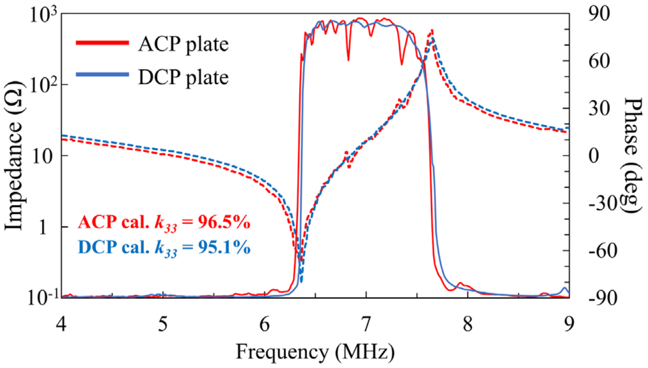

Fig. 4. (Color online) The impedance spectra of PMN-30.5PT SC plate vibrators by ACP and DCP.

phase. However, it is difficult to estimate whether PMN-0.305PT is M_A phase or M_B phase after ACP only by XRD, which is a subject to be solved in the future.

4. Conclusion

The [001]-oriented PMN-0.305PT SC manufactured by a conventional one charge Bridgman process with giant piezoelectric constant d_{33} of 4200 pCN^{-1} and dielectric permittivity of 14500 after 100 h was successfully obtained by ACP technology. And the calculated coupling coefficient k_{33} was up to 96.5% of the plate sample. These values are the highest ever reported. Although the SC plate showed excellent properties, these 0.15 mm width silver mode vibrators diced from the SC plate showed many small spurious mode

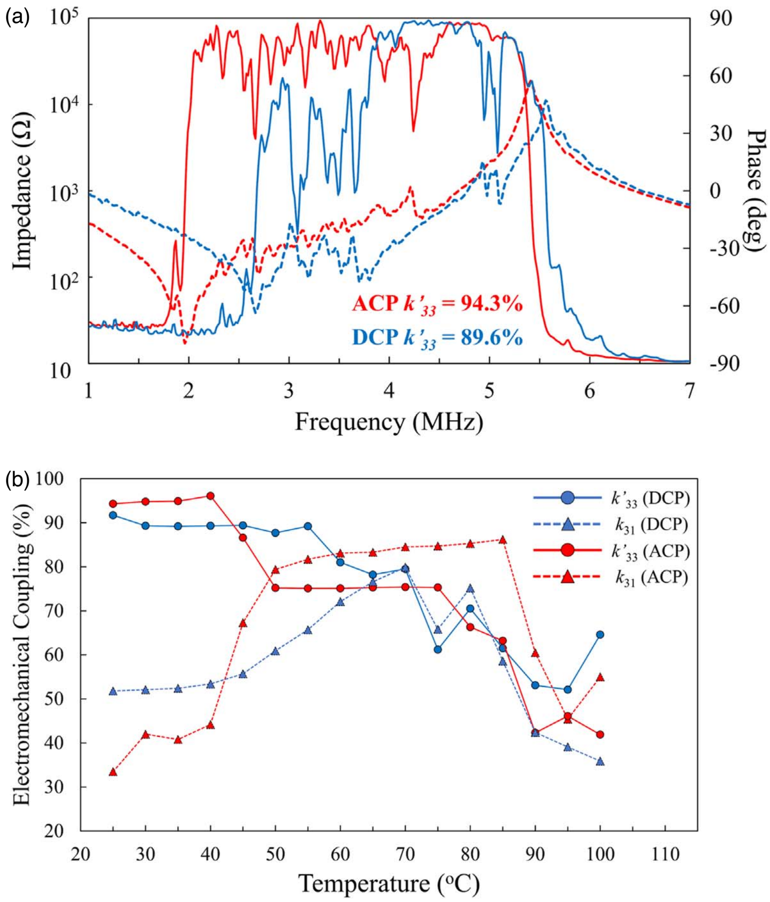

Fig. 5. (Color online) (a) The impedance spectra of PMN-0.305PT silver mode vibrators by ACP and DCP. (b) The coupling coefficient k_{31} and k'_{33} of silver mode vibrators by ACP and DCP with temperature increasing.

Table II. Dielectric and piezoelectric properties of the rectangular plates and silver mode vibrators of the PMN-0.305 PT SC after ACP and DCP.

Sample	DCP plate	ACP plate	Difference	DCP silver	ACP silver	Difference
$\varepsilon_{33}^T/\varepsilon_0$ at 25 °C	9700	14500	+(49%)	4190	6750	+(61%)
tan δ at 25 °C (%)	0.32	0.33	+(3%)	0.49	0.37	−(24%)
$\varepsilon_{33}^S/\varepsilon_0$ at 25 °C	910	1030	+(13%)	870	1130	+(30%)
T_{RT} (°C)	77.0	66.9	−(13%)	/	/	/
T_C (°C)	142.3	142.8	0%	/	/	/
$\varepsilon_{33}^T/\varepsilon_0$ at T_{RT}	23200	38700	+(67%)	/	/	/
$\varepsilon_{33}^T/\varepsilon_0$ at T_C	42700	48100	+(13%)	/	/	/
tan δ at T_{RT} (%)	1.35	1.18	−(13%)	/	/	/
tan δ at T_C (%)	1.36	1.13	−(16%)	/	/	/
d_{33} (pCN^{-1})	2750	4200	+(53%)	1300	2200	+(69%)
k_t (%)	59.3	59.5	0%	/	/	/
calculated k_{33}	95.0	96.5	2%	90.4	91.2	+(1%)
k'_{33} (%)	/	/	/	89.6	94.3	+(5%)

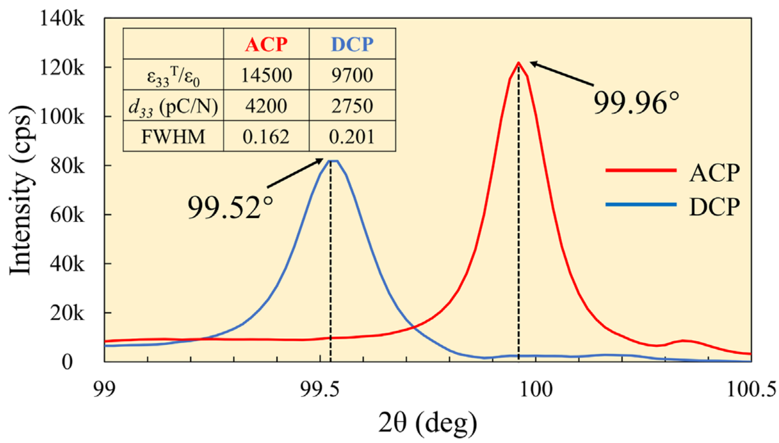

Fig. 6. (Color online) The XRD result of (004) face for PMN-0.305PT plate sample by ACP and DCP.

vibrations on its impedance spectra near the fundamental thickness mode which are very different to eliminate.

The PMN-0.305PT SC plate near MPB shows excellent piezoelectric and dielectric properties, however, these silvers tend to show SMV after dicing. This information is useful to select optimal PMN-*x*PT composition for medical array probe application.

According to XRD result of PMN-0.305PT (004) surface, we presumed that ACP can eliminate the 71° domain walls of PMN-0.305PT, indicating that the 109° domain walls should be the most stable in $[001]_C$-poled monoclinic PMN-PT SCs

ORCID iDs

Yiqin Sun https://orcid.org/0000-0002-6183-8654

1) S. E. Park and T. R. Shrout, J. Appl. Phys. **82**, 1804 (1997).
2) S. Zhang and F. Li, J. Appl. Phys. **111**, 031301 (2012).
3) E. Sun and W. Cao, Prog. Mater Sci. **65**, 124 (2014).
4) S.-E. Park and T. R. Shrout, IEEE Trans. Ultrason. Ferroelectr. Freq. Control **44**, 1140 (1997).
5) T. R. Shrout, Z. P. Chang, N. Kim, and S. Markgraf, Ferroelectr. Lett. **12**, 63 (1990).
6) Y. Guo, H. Luo, D. Ling, H. Xu, T. He, and Z. Yin, J. Phys. Condens. Matter **15**, L77 (2003).
7) H. Fu and R. E. Cohen, Nature **403**, 281 (2000).
8) J. Li, J. Li, H.-H. Wu, O. Zhou, J. Chen, T. Lookman, Y. Su, L. Qiao, and Y. Bai, ACS Appl. Mater. Interfaces **13**, 38467 (2021).
9) F. S. Foster, C. J. Pavlin, K. A. Harasiewicz, D. A. Christopher, and D. H. Turnbull, Ultrasound Med. Biol. **26**, 1 (2000).
10) F. S. Foster, G. R. Lockwwod, L. K. Ryan, K. A. Harasiewicz, L. Berube, and A. M. Rauth, IEEE Trans. Ultrason. Ferroelectr. Freq. Control **40**, 608 (1993).
11) D. W. Wu, R. M. Chen, Q. F. Zhou, K. K. Shung, D. M. Lin, and H. L. W. Chan, Ultrasonics **49**, 395 (2009).
12) P. N. T. Wells, IEEE Eng. Med. Biol. **19**, 14 (2000).
13) N. Yamamoto, Y. Yamashita, Y. Hosono, and K. Itsumi, Sens. Actuator A Phys. **200**, 16 (2013).
14) Y. Chen et al., Sensors **14**, 13730 (2014).
15) J. Chen and R. Panda, IEEE. Ultrason. Symp. **1**, 235 (2005).
16) N. Yamamoto, Y. Yamashita, Y. Hosono, K. Itsumi, and K. Higuchi, U.S. Patent Application Publication 2014/0062261 A1 (2014).
17) Y. Yamashita, N. Yamamoto, Y. Hosono, and K. Itsumi, U.S. Patent Application Publication 2015/0372219 A1 (2015).
18) J. Xu et al., Appl. Phys. Lett. **112**, 182901 (2018).
19) C. Qiu, J. Liu, F. Li, and Z. Xu, J. Appl. Phys. **125**, 014102 (2019).
20) W.-Y. Chang, C.-C. Chung, C. Luo, T. Kim, Y. Yamashita, J. L. Jones, and X. Jiang, Mater. Res. Lett. **6**, 537 (2018).
21) Z. Zhang, J. Xu, L. Yang, S. Liu, J. Xiao, R. Zhu, X. Li, X. Wang, and H. Luo, J. Appl. Phys. **125**, 034104 (2019).
22) H. Wan, C. Luo, W.-Y. Chang, Y. Yamashita, and X. Jiang, Appl. Phys. Lett. **114**, 172901 (2019).
23) Y. Sun, T. Karaki, T. Fujii, and Y. Yamashita, Jpn. J. Appl. Phys. **58**, SLLC06 (2019).
24) C. He, T. Karaki, X. Yang, Y. Yamashita, X. Sun, and Y. Long, Jpn. J. Appl. Phys. **58**, SLLD06 (2019).
25) C. Luo, H. Wan, W.-Y. Chang, Y. Yamashita, A. R. Paterson, J. Jones, and X. Jiang, Appl. Phys. Lett. **115**, 192904 (2019).
26) C. Qiu et al., Nature **577**, 350 (2020).
27) C. Luo, T. Karaki, Y. Sun, Y. Yamashita, and J. Xu, Jpn. J. Appl. Phys. **59**, SPPD07 (2020).
28) Y. Sun, T. Karaki, T. Fujii, and Y. Yamashita, Jpn. J. Appl. Phys. **59**, SPPD08 (2020).
29) M. Ma, S. Xia, K. Song, H. Guo, S. Fan, and Z. Li, J. Appl. Phys. **127**, 064106 (2020).
30) L. Guo, B. Su, C. Wang, X. He, Z. Wang, X. Yang, X. Long, and C. He, J. Appl. Phys. **127**, 184104 (2020).
31) J. Xu et al., Appl. Phys. Lett. **116**, 202903 (2020).
32) J. Liu, C. Qiu, L. Qiao, K. Song, H. Guo, Z. Xu, and F. Li, J. Appl. Phys. **128**, 094104 (2020).
33) Z. Zhang, J. Xu, S. Liu, J. Xiao, X. Wang, Z. Liang, and H. Luo, Ultrasonics **108**, 106175 (2020).
34) C. Luo, T. Karaki, Y. Yamashita, and J. Xu, J. Materiomics. **7**, 621 (2021).
35) Y. Sun, T. Karaki, Z. Wang, T. Fujii, and Y. Yamashita, Jpn. J. Appl. Phys. **60**, SFFC04 (2021).
36) C. Luo, T. Karaki, Z. Wang, Y. Sun, Y. Yamashita, and J. Xu, J. Adv. Ceram. **11**, 57 (2022).
37) F. Li et al., Science **364**, 264 (2019).
38) H. Wan, C. Luo, H.-P. Kim, C.-C. Chung, W.-Y. Chang, Y. Yamashita, and X. Jiang, Appl. Phys. Lett. **120**, 192901 (2022).
39) D. Shimizu, S. Tsukada, M. Matsuura, J. Sakamoto, S. Kojima, K. Namikawa, J. Mizuki, and K. Ohwada, Phys. Rev. B **92**, 174121 (2015).
40) C. Qiu, Z. Xu, Z. An, J. Liu, G. Zhang, S. Zhang, L.-Q. Chen, N. Zhang, and F. Li, Acta Mater. **210**, 116853 (2021).
41) H. Wan, C. Luo, C.-C. Chung, Y. Yamashita, and X. Jiang, Appl. Phys. Lett. **118**, 102904 (2021).

